Journal of Materials Chemistry C

Accepted Manuscript

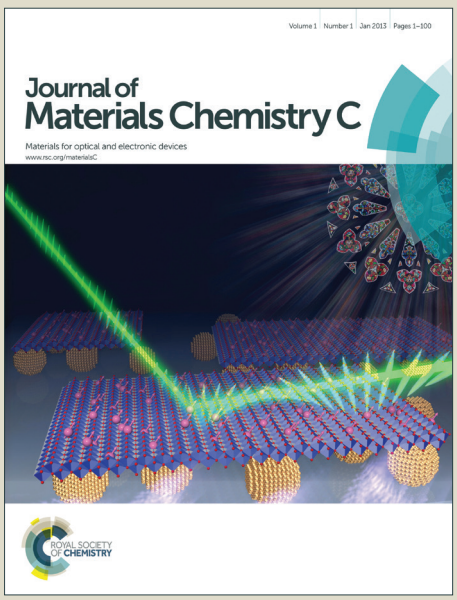

ROYAL SOCIETY OF CHEMISTRY

www.rsc.org/materialsC

Journal of Materials Chemistry C

RSCPublishing

ARTICLE

Synthesis and optical properties of iron(III) complexes of 2-benzylidene-1-indanone derivative thin films

Cite this: DOI: 10.1039/xoxxoooooox

M. Lozano González[a], M. E. Sánchez-Vergara[b*], J. R. Álvarez[b], Ma. I. Chávez-Uribe[a], Rubén A. Toscano[a], C. Álvarez-Toledano[a]*

Received ooth March 2014,
Accepted ooth January 2012

DOI: 10.1039/xoxxoooooox

www.rsc.org/

In this work, we propose a different method to synthetize 2-benzylidene-1-indanone derivatives and a new method to obtain iron(III) complexes of 2-benzylidene-1-indanone derivatives, used to prepare semiconducting thin films. The 2-benzylidene-1-indanones derivatives were obtained from the reaction of *o*-phthalaldehyde with acetophenone in a basic medium and were later complexed with $Fe_2(CO)_9$ to form iron(III) complexes from the corresponding redox reaction. One of the iron complexes (**4a**) was fully characterized by single-crystal X-ray diffraction. Iron(III) complexes of 1-indenol derivative thin films were obtained by thermal evaporation in a high vacuum source. All the samples were grown at room temperature (25°C) and low deposition rates (0.2 Å/s) on quartz substrates and (100) single-crystalline silicon (c-Si) wafers. The surface morphology and structure of the deposited films were studied by atomic force microscopy (AFM) and scanning electron microscopy (SEM). Optical absorption studies of the iron(III) complex films were performed in the 100-1150 nm wavelength range. The optical band gap (E_g) of the thin films was determined from the $(\alpha h\nu)^{1/2}$ vs. $h\nu$ plots for indirect allowed transitions. The iron(III) complex films show optical activation energies around 2.1 eV, depending on the 1-indenol derivative. From these results, iron complexes of 1-indenol derivatives may prove suitable for photovoltaic or luminescence applications.

***Keywords*:** Chemical synthesis; thin films; optical properties; electrical properties

Introduction

The search for new materials for optoelectronic applications has led to an ever increasing interest in organometallics and organic compounds. Compounds combining different organometallic moieties and their electron transfer processes have attracted considerable attention [1-3]. Organometallic compounds may eventually be considered for electronics applications requiring large area coverage, structural flexibility and low-temperature processing [4-6]. Recent research work has been oriented to the formation and characterization of semiconducting thin films. Some methods have been extensively used to produce organometallic semiconducting thin films, such as chemical vapor deposition, electrodeposition and vacuum thermal evaporation [7]. Research on the production of films with transition metal complexes has particular relevance, due to the oxidation states of transition metals by the electron transfer processes. Metal chelates are one of these transition metal complexes that are widely used as building blocks in modern organic synthesis. A thorough understanding of their structure and reactivity is important because many of these compounds exist as aggregates in solutions and in the solid state. Depending on the metal and organic building blocks, they can possess properties such as luminescence, catalytic capability and other material chemical features [8]. These metal chelates with oxygen atoms, such as β-diketones, can form transition metal complexes with atoms like gadolinium that show interesting luminescent properties [8].Other organic building blocks worthy of consideration are 2-hydroxyphenone, indenols and 2-benzylidene-1-indanones.

There are spectroscopic investigations of arylidene derivatives that show that an increase in the electron interactions of electron-donor substituents in a conjugated bond system leads to some kind of flattening of the molecules [9], so this feature in 2-benzylidene-1-indanone is an interesting structural characteristic for materials chemistry applications. As far as we are aware, there are no reports of this phenomenon involving the preparation of semiconducting thin films with iron.

1-indanone compounds are important synthetic intermediates for pharmaceutical agents and biologically active compounds, and there are numerous methods available for the preparation of 1-indanones [10a]. Akio Saito *et al.* described their synthesis with catalytic SbF_5 and the use of EtOH to convert a mixture of phenylalkynes and aldehydes to indanone compounds in one pot. [10a]. The benzylidene-1-indanone derivatives have many conjugated unsaturated linkages, so they are versatile building blocks for many compounds, such as pharmaceuticals, agrochemicals and perfumes, new organic materials for nonlinear optical applications, cytotoxic analogs, and the units of liquid-crystalline polymers [10b]. Many molecules of this type are synthesized from aldehydes and cycloalkanones. Yu Wan *et al*. synthesized α,α'Bis(substituted-benzylidene)cycloalkanones via a solvent-free cross-aldol

condensation of aromatic aldehydes with cycloalkanones in the presence of a catalytic amount of 1-methyl-3(2-(sulfooxy)ethyl)-1H-imidazol-3-ium chloride at room temperature and showed their optical properties [10b]. Camille Carrignon et al. obtained α,α'Bis(substituted-benzylidene)cycloalkanone derivatives using chloride ion pairs as catalysts for the alkylation of aldehydes and ketones with C-H acidic compounds [10c].

In this work, we propose an easier and faster method to synthesize 2-benzylidene-1-indanone derivatives and a new method to synthetize iron(III) complexes of 2-benzylidene-1-indanone derivatives. Thin films of these complexes were prepared by thermal evaporation and characterized by scanning electron microscopy (SEM), atomic force microscopy (AFM) and infrared spectroscopy (IR). We also report the determination of optical parameters related to the main transitions in the UV-Vis region, as well as the fundamental energy gap calculations for these films.

Results and discussion

In this work, we used carbonyl-substituted 2-benzylidene-1-indanone, *o*-phthalaldehyde and aryl-substituted methyl ketones with a sodium hydroxide ethanolic solution at room temperature, which provided good yields and a faster reaction. To understand the influence of different substituents in this type of compounds in the presence of $Fe_2(CO)_9$, 2-benzylidene-1-indanone derivatives were synthesized according to the reaction shown in Figure 1.

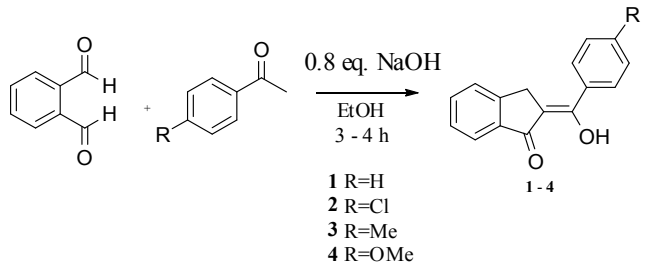

Figure 1. Synthesis of 2-benzylidene-1-indanone derivative compounds **1** to **4**.

The IR spectra of the substituted 2-benzylidene-1-indanone derivatives **1-4** showed the characteristic absorption assigned to the C=O group vibrations near 1700 cm^{-1}, and the absence of absorption in the ν(O-H) region in 2-benzylidene-1-indanone spectrum was considered evidence that the free ligand is a proton chelate and therefore exists largely in the chelated enol form [11]. The analysis of the NMR spectroscopic data (^1H, ^{13}C, COSY, HSQC and HMBC experiments) allowed to discern between the two possible enolic forms (Figure 2a and b), according to the location of the double bond (endocyclic or exocyclic to the ring B) in solution (Figure 2).

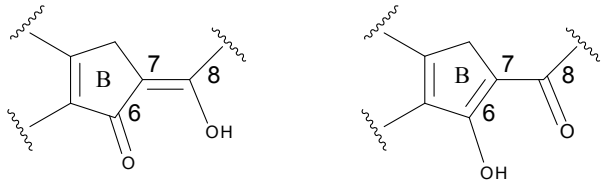

Figure 2. a) Exocyclic double bond, 2-benzylidene-1-indanone-type and b) endocyclic double bond, 1-indenol-type.

The 1H and 2D COSY experiments showed a characteristic AA'BB' system which corresponded to the hydrogen atoms H-1, H-2, H-3 and H-4 of ring A, and a second aromatic system was assigned to the hydrogen atoms H-10 to H-14 for ring C. At 3.8-3.9 ppm resonated a singlet which integrated for two hydrogens that were assigned to H-15a,b of ring B. The HSQC experiments allowed the identification of the corresponding carbons linked to the hydrogens described above, confirming the assignments. In the ^{13}C spectra for compound **1** and for compounds **2** – **4,** three and four signals of quaternary aromatic carbons were observed, respectively. These were assigned to C-5, C-16 of ring A and C-9 and C-12 of ring C, since HMBC correlations were observed (Figure 3) between H-2 and C-16, between H-3 and C-5, and between H-10, H-11, H-13 and H-14 with C-9 and C-12. Finally, long range HMBC correlations established the location of the double bond at C7-C8 for compounds **1** - **4**, according to the following observations: the aromatic hydrogen H-4 displayed HMBC cross-peak with the carbonyl C-6 (194.5-196 ppm); the aromatic hydrogen H-1 correlated with the methylene C-15, and the aromatic hydrogens H-10 and H-14 correlated with the olefinic carbon C-8. The same correlations were observed for compounds **1-4**, confirming the structures.

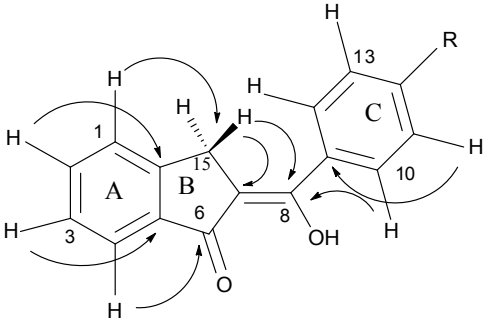

Figure 3. HMBS correlations of **1** to **4**

Crystals suitable for the X-ray structure determination of compound **1** were grown from a mixture of *n*-hexane and dichloromethane solution that confirmed the structure proposed (Figure 4). **1** crystallizes in the space group $Pna2_1$ with two symmetry independent molecules in the unit cell, A and B. In both symmetry independent molecules, the bond C–O of carbonyl 1.274 (14) and 1.16(3) and hydroxyl 1.437(19) and 1.35(2) show a good differentiation of both moiety groups that correlates with the RMN experiments. The crystal forms a two-dimensional, hydrogen-bonded (O-H---O), network, which is parallel to the plane, and the enol form is stabilized through an intramolecular hydrogen. Details of the collected crystallographic data are provided in ESI.

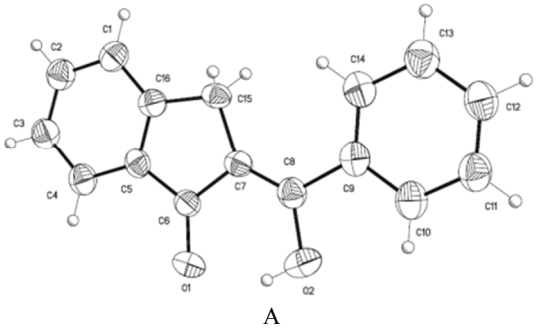

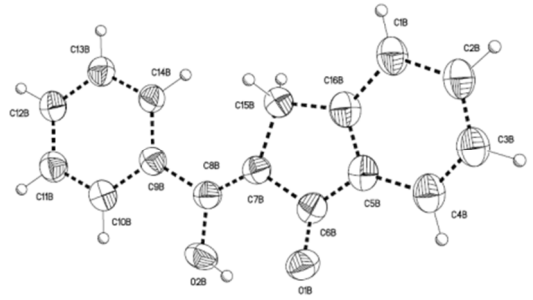

B

Figure 4.ORTEP plot of the two symmetry-independent molecules of **1**. Atomic labels are shown for the asymmetric units and hydrogen atoms have been omitted for clarity.

These results show that the generalization made by Brown is correct in this case: "*Double bonds which are exo to a 5-ring are less reactive and more stable than related double bonds which are exo to a 6-ring. Reactions which involve the formation or retention of an exo double bond in a 5-ring derivative will be favored over corresponding reactions which involve the formation or retention of an exo double bond in a 6-ring derivative*" [12].

A suspension of ligands **1**-**4** and $Fe_2(CO)_9$ in anhydrous ether (Figure 5) led to the formation of **1a**-**4a,** which were isolated by filtration. As far as we are aware, there are no reports of the synthesis of **1a**-**4a** by other methods. Paramagnetic complexes **1a**, **2a**, **3a**, **4a** were obtained as violet, deep red and black crystalline solids.

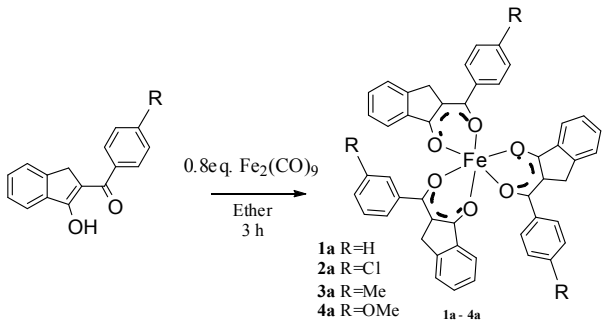

Figure 5. Synthesis of iron complexes of 2-benzylidene-1-indanone derivative compounds **1a** to **4a**

Crystals suitable for the X-ray structure determination of **4a** were grown from a mixture of *n*-hexane and dichloromethane solution (Figure 6). Details of the collected crystallographic data are provided in ESI. Complex **4a** crystallizes in the space group R-3. The molecular structure is shown in Figure 3 and confirms the suggested structure. The units show a distorted octahedral arrangement (Table 1), with the *trans* O-Fe-O angles of 175.07(11)º, and very similar *cis* O-Fe-O angles which fall in the range 86.75(11)-92.53(11)º. The corresponding Fe-O distances of hydroxyl (1.98 Å) and carbonyl are very similar (1.99 Å). This arrangement follows a trend that was observed in some complexes formed by iron(III) with salicylate-based tripodal ligands [13]. The rest of the synthesized compounds (**1a**-**3a**) are expected to have a similar crystalline structure because the only change in the compound refers to the radical of the iron complex.

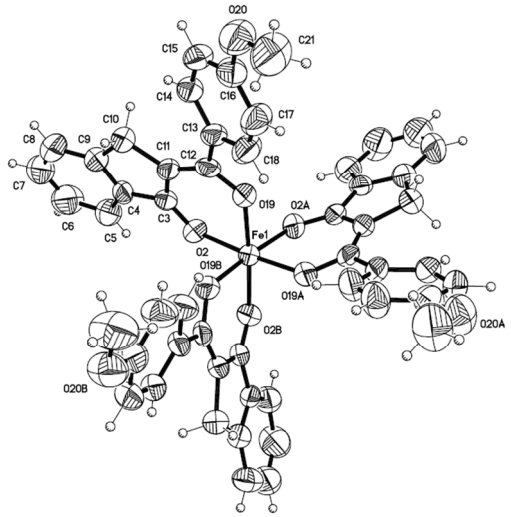

Figure 6.ORTEP drawing, with omission of hydrogen atoms, of the complex **4a.**

Table 1. Selected interatomic distances (Å) and angles (°) for **4a**

Bond	(Å)	Angle	(°)
Fe1-O19	1.983 (3)	O19-Fe1-O19 (1)	88.45 (11)
Fe-O2	1.999 (3)	O19(1)-Fe1-O2	175.08 (11)
O2-C3	1.281 (4)	O19-Fe1-O2	86.75 (11)
O2-C2	1.297 (4)	O19-Fe1-O2 (1)	92.53 (10)
		O19-Fe1-O2(2)	175.07 (11)

IR analysis shows some similarities in the IR spectrum absorption bands for the compounds **1a** to **4a** (see Table 2). Absence of absorption in the 1700 cm^{-1} region was construed as evidence that coordination occurs through the enol tautomer. Features in the region around 1580-1600 cm^{-1} were attributable to the carbonyl bond ν(C=O), that is shifted to lower frequencies; this and the presence of the band around 1550 cm^{-1}, attributable to the C-O bond of increased single-bond order, were consistent with a cyclic structure for the metal complexes with coordination through both carbonyl groups [13].

Table 2. IR (cm^{-1}) characteristic bands for powder and thin films

Compound	ν(C=O) cm^{-1}	ν(C-O) cm^{-1}
1a (pellet)	1587	1553
1a (thin film)	1584	1552
2a (pellet)	1582	1551
2a (thin film)	1580	1553
3a (pellet)	1585	1546
3a (thin film)	1582	1550
4a (pellet)	1599	1547
4a (thin film)	1595	1549

After deposition of the thin films, a comparison of the IR absorption spectra of the synthesized complexes and those of the deposited films indicated that thermal evaporation is a good technique to obtain iron complexes of 2-benzylidene-1-indanone derivative thin films [8] Iron(III) in 2-benzylidene-1-indanone derivatives can form complexes with strong metal-ligand covalent bonds, which enhance

molecular stability and support the sublimation process without dissociation [8]. The IR measurements were performed on films deposited over monocrystalline silicon substrates. There are few differences between signals identified on powder materials and those deposited on films, and they may be due to internal stress produced during the vaporization process.

The variations in the microscopic morphology and roughness of the films deposited onto quartz substrates were examined by atomic force microscopy and are shown in Figure 7 and Table 3. 3D micrographs provide a large surface inspection of the micro-structural arrays, topological structure, porosity and film quality of the deposited layers. Thin films from samples **1a**, **2a** and **4a** (Figures 7a/b and 7d) show a very similar aspect. The films are extremely homogeneous and a fine granular structure can be observed in them. In the case of the film from sample **3a**, a heterogeneous distribution is seen and particles agglomerate to generate irregular structures (Figure 7c). The calculated RMS wrinkle heights for the thin films are shown in Table 3. This evaluation was performed on three different sites. The difference in the roughness values may be related to the different iron(III) complexes of 2-benzylidene-1-indanone derivatives in each thin film. Less roughness is found in the compound with hydrogen **1a** and in the complex **4a** with the methoxy group, while thin film **2a** with Cl and thin film **3a** containing the methyl group as a substituent are the roughest. In fact, compound **3a**, with the methyl group, produces the most heterogeneous and roughest thin film, followed by compound **2a**, with the chloride anion. The methyl- and chloride-containing compounds seem to have been most affected by the thermal gradient occurring between the room-temperature substrate and the high-temperature evaporated material, which nucleated upon the substrate and then completely covered it during the sublimation process. IR spectroscopy results suggest that the compounds did not undergo chemical decomposition (Table 2) and had similar deposition rates. Nevertheless, they showed –as thin films– morphological differences that depended directly on the substituent radical and the electrostatic forces occurring during deposition.

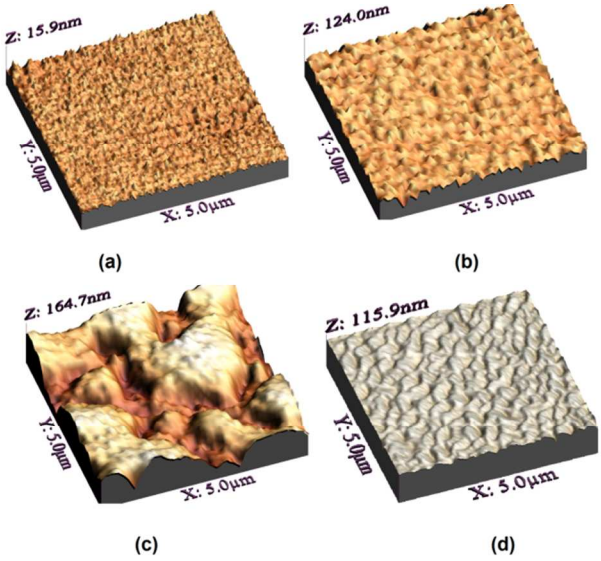

Figure 7. 3D-micrographs obtained by AFM, showing the surface morphology of thin films deposited on quartz slices from the: (a) **1a** thin film, (b) **2a** thin film, (c) **3a** thin film and (d) **4a** thin film, respectively.

Table 3. AFM evaluation of the thin film roughness, thickness and optical activation energy

Compound	RMS roughness (nm)	Film thickness (Å)	Indirect optical activation energy (eV)
1a	1.29	959	2
2a	29.06	1527	2.1
3a	33.45	1233	2.1
4a	4.57	3632	2.1

The SEM micrographs in Figure 8 show the surface morphologies of iron(III) complexes of 2-benzylidene-1-indanone derivatives; notice the small domains. Figures 8a, 8b and 8d show micrographs at 1000x corresponding to the **1a**, **2a** and **4a** thin films, respectively. From these figures, it is clear that the evaporation process (with the substrate at 323 K) produced homogeneous thin films. In the 1000x micrograph of the **3a** thin film (Figure 8c), one can readily find two apparent phases. One phase shows a coating with elongated crystals and the second one is the homogeneous phase. Although this film was grown at room temperature and low deposition rates, we observe a significant contribution of the bulk crystalline phase, with seemingly preferential directions for crystal nucleation and growth. This effect may be attributed to the higher thickness of the thin film [5]. Table 3 shows thickness values for all thin films. It is worth noting that the most heterogeneous deposition, as well as the roughest thin film, corresponds to the compound having a methyl functional group in its molecule. This film feature seems to be a consequence of its particular crystal growth.

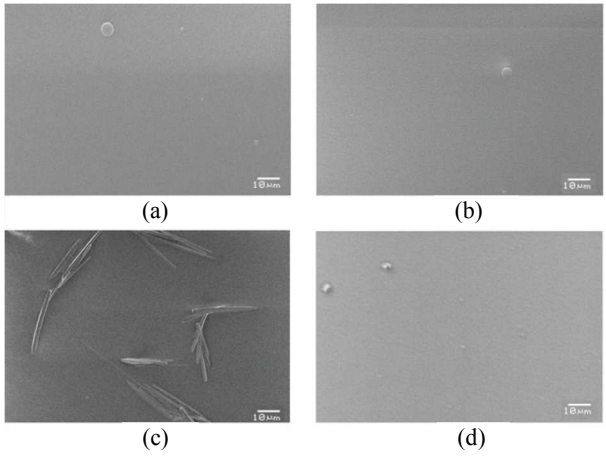

Figure 8. SEM micrographs of materials (a)1a, (b)2a, (c)3a and (d) 4a, at 1000x.

UV spectra of iron(III) complexes of 2-benzylidene-1-indanone derivatives show high-intensity bands arising from electronic transitions in the conjugated system (see Figure 9a). The iron(III) complexes of 2-benzylidene-1-indanone derivatives have absorption bands in the UV-visible region assigned to the following electronic transitions: (i) d-d transitions arising from ligand field interactions, (ii) intraligand transitions ($\pi \rightarrow \pi^*$) arising from molecular orbitals localized in the ligand and (iii) charge transfer transitions (LMCT or

MLCT) involving an electron transition from the ligand to the metal ion or from the metal ion to the ligand, respectively [8]. An intense band appearing in the near-ultraviolet region (228 - 241 nm) seems to correspond to a $\pi \rightarrow \pi^*$ transition in the enolate ring [8] and the one at 276 – 297 nm comes from $\pi \rightarrow \pi$ and $\pi \rightarrow \pi^*$ intraligand transitions. The band around 410-422 nm is due to charger transfer from the ligand to the metal ion [8]. The π interaction in the enolate ring is influenced by the type of ligand substituent; hence, the spectral differences found for each film [14]. Figure 9b shows the UV-vis ligand and complex spectra. The absence of the signal at about 400 nm in the ligand spectrum is readily noticed, suggesting substantial changes in electron mobility arising from the addition of the metallic ions. From the obtained absorption values, use of these films as photoconducting materials and in color filters may be considered [15].

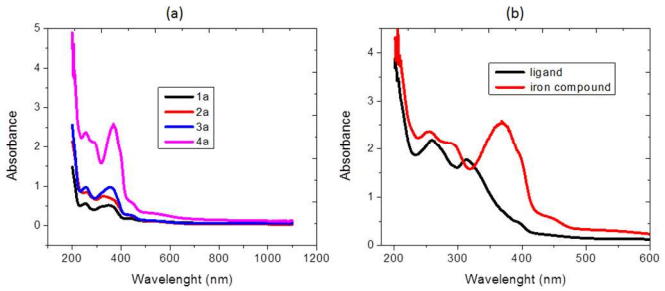

Figure 9. a) UV spectra of iron(III) complexes of 2-benzylidene-1-indanone derivatives b) UV spectra of ligand and iron compound 4 and 4a

The value of the absorption coefficient (α) of iron(III) complexes of 2-benzylidene-1-indanone derivative thin films is calculated at different energies and plotted in Figure 10a. Up to about 3 eV, α has a similar value in all the compounds. This may be due to the absorption coefficient explicitly depending on the electronic structure of the metal ion. The peak at the UV threshold indicates the contribution of the d-electrons of the iron(III) to the electronic transitions [16a-b]. For higher energy values, however, the **3a** thin film (the one with methyl) has the largest α value, while the **2a** film (the one with chloride) has the smallest α. Methyl's electronic density and the film's heterogeneity also affect the material's optical behavior at higher photon energies (*hv*). Notice, however, that thin-film optoelectronic applications frequently involve *hv* values smaller than 2 eV. To obtain information on direct or indirect inter-band transitions, the fundamental absorption edge data was analyzed within the framework of one-electron theory [16a-b] and according to the relation:

$$\alpha = \alpha_0(hv - E_g)^r$$

E_g is the optical band gap, and r determines the type of transitions, with r = 2 and 3 for allowed and forbidden indirect transitions and r =1/2 and 3/2 for allowed and forbidden direct transitions. The dependence of $(\alpha)^{1/r}$ on photon energy (*hv*) was evaluated and plotted for different values of r, and the best fit was obtained for r = 2. This characteristic behavior corresponds to allowed indirect transitions [16a-b]; the optical band gap is determined from the intercept on the energy axis of the linear fit of the larger energy data, in a plot of $(\alpha hv)^{1/2}$ vs *hv* (Tauc extrapolation [17]), as shown in Figure 10b. The optical gap for **1a**-**4a** was found to be in the range 2-2.1 eV (see Table 3), corresponding to wavelengths of 590-620 nm in the electromagnetic spectrum. The non-direct electronic transitions seem to be of the π to π^* type. In these electronic transitions, occurring from states of the valence band to states of the conduction band, there is no conservation of the electronic momentum [18]. The optical activation energy values are very similar in all the compounds. The ligand does not seem to influence electronic transport between the valence and conduction bands of these compounds, the metallic center being responsible for conductivity. From these results, iron(III) complexes of 2-benzylidene-1-indanone derivatives may prove suitable for photovoltaic [18] or luminescence applications [8], as well as in dyes and pigments. Their semiconductor-like properties may also permit their use in sensors and molecular electronics applications. As the metallic ion and its oxidation state are the main drivers of the optical properties in these thin films, the effect of other metallic atoms in the ligand needs to be understood in order to better establish a specific application for these materials. Work with complexes involving other metals has now been undertaken and will be published later on.

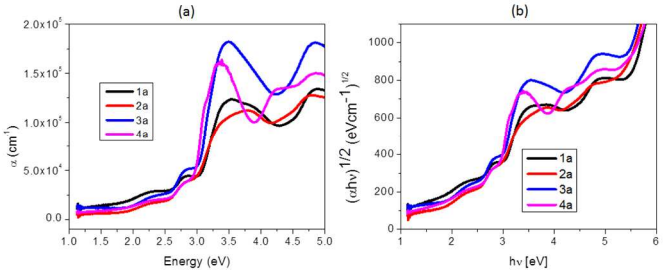

Figure 10. a) Energy dependence of the absorption coefficient (α) of iron(III) complexes of 2-benzylidene-1-indanone derivative thin films b) Plot of $(\alpha/hv)^{1/2}$ vs. photon energy *hv*.

Experimental

All reagents and solvents were obtained from commercial suppliers and used without further purification. $Fe_2(CO)_9$ was synthesized from $Fe(CO)_5$ according to the literature [12]. All compounds were characterized by IR spectra, recorded on a Perkin-Elmer 283B or 1420 spectrophotometer, by the KBr technique, and all data are expressed in wavenumbers (cm^{-1}). Melting points were obtained on a Melt-Temp II apparatus and are uncorrected. Nuclear magnetic resonance spectra were recorded with a Bruker AV 400 or JEOL Eclipse +300 spectrometer. Chemical shifts for the ^1H NMR spectra were recorded in parts per million from tetramethylsilane with the solvent resonance as the internal standard (chloroform, δ = 7.25 ppm). Chemical shifts for the ^{13}C NMR spectra were recorded in parts per million from tetramethylsilane using the central peak of $CDCl_3$ (δ = 77.1 ppm) as the internal standard. Mass spectra were recorded with a JEOL JMSAX 505 HA spectrometer at 70 eV using the electronic impact (EI) and fast atom bombardment (FAB^+) technique. A suitable X-ray-quality crystal of one of the iron complexes (**4a**) was grown by slow evaporation of an *n*-hexane-CH_2Cl_2 mixture at room temperature. The crystal was mounted on a glass fiber at room temperature, and then placed on a Bruker Smert Apex CCD diffractometer, equipped with Mo Kα radiation; decay was negligible. Structure solutions and refinements were performed using SHELXTL V6.10 [19].

General procedure for the synthesis of 2-benzylidene-1-indanone derivatives. The reaction between *o*-phthalaldehyde and acetophenone in a basic medium was performed to produce the 2-benzylidene-1-indanone type compound under simpler and faster conditions. *O*-Phthalaldehyde was added slowly to a cool sodium hydroxide (0.8 eq.) ethanolic solution with the appropriate amount of acetophenone. The reaction mixture was stirred at room temperature for approximately 3 h, and then poured into a mixture of ice and commercial hydrochloric acid (pH was adjusted to about 7). The

resulting solid was filtered and in some cases purified by column chromatography using hexane/ethyl acetate.

Compound 1 ($C_{16}H_{12}O_2$, *M*=236 g/mol) was prepared starting from *o*-phthalaldehyde (0.5 g, 3.7 mmol), acetophenone (0.48g, 3.7 mmol) and NaOH (0.119 g, 2.98 mmol) and was obtained as a yellow solid, **mp**. 90°C, (0.67g, 2.82 mmol, 75%). **IR**: ν 1604, 1564 cm^{-1}. **^{1}H NMR** (300 MHz, $CDCl_3$): δ= 15.067(s, 1H, OH), 7.49, 7.5(d, 1H, 1), 7.54 (ddd, 1H, 2), 7.40 (dd,1H,3), 7.85(d, 1H, 4), 7.91(m, 1H,10), 7.48 (m,3H,11,12,13), 7.91(m, 1H,14), 3.86 (sa, 2H, 15) ppm. **^{13}C NMR** (75MHz, $CDCl_3$): δ = 125.54 (C1), 133.27 (C2), 127.40 (C3), 123.36 (C4), 137.85 (C5), 195.70 (C6), 109.41 (C7), 170.79 (C8), 134.79 (C9), 128.07 (C10), 128.55 (C11), 131.21 (C12), 128.55 (C13), 128.07 (C14), 32.19 (C15), 148.51(C16) ppm. **MS (EI):** m/z (%) = 236 (1.9%). **HRMS** (FAB^+): calculated for $C_{16}H_{12}O_2$: 237.0821. Found: 237.0823.

Compound 2 ($C_{16}H_{11}ClO_2$, *M*=270.5 g/mol) was prepared starting from *o*-phthalaldehyde (0.5 g, 3.7 mmol), 4'-chloroacetophenone (0.58g, 3.7 mmol) and NaOH (0.119g, 2.98 mmol) and was obtained as a pale brown solid, mp. 162-164°C, (0.8g, 2.96 mmol, 80%). **IR**: ν 1605, 1559 cm^{-1}. **^{1}H NMR** (300 MHz, $CDCl_3$): δ= 15.03 (s, 1H, OH), 7.54 (d, 1H9, 1), 7.60 (d, 1H, 2), 7.44 (ddd, 1H, 3), 7.86 (dd, 1H, 4), 7.89 (d, 2H, 10,14), 7.48 (d, 2H, 11,13), 3.91 (s, 2H, 15) ppm. **^{13}C NMR** (75MHz, $CDCl_3$): δ = 125.45 (C1), 133.35 (C2), 127.35 (C3), 123.19 (C4), 137.44 (C5), 195.63 (C6), 109.29 (C7), 169.14 (C8), 132.99 (C9), 129.22 (C10), 128.70 (C11), 137.22 (C12), 128.70 (C13), 129.22 (C14), 31.95 (C15), 148.19 (C16) ppm. **MS (EI):** m/z (%) = 270 (15%). **HRMS** (FAB^+): calculated for $C_{16}H_{11}ClO_2$: 271.0526. Found: 271.0522.

Compound 3 ($C_{17}H_{14}O_2$, *M*=250 g/mol) was prepared starting from *o*-phthalaldehyde (0.5 g, 3.7 mmol), 4'-methylacetophenone (0.5g, 3.7 mmol) and NaOH (0.119g, 2.98 mmol) and was obtained as a yellow solid, **mp**. 96-98°C, (0.71g, 2.84 mmol, 76 %). **IR:** ν 1604, 1540 cm^{-1}. **^{1}H NMR** (300 MHz, $CDCl_3$): δ= 15.17 (s, 1H, OH), 7.50 (d, 1H, 1), 7.55 (ddd, 1H, 2), 7.41 (dd, 1H, 3), 7.85(d, 1H, 4), 7.84 (d, 1H, 10), 7.30 (d, 2H, 11,13), 7.84 (d, 1H, 14), 3.89 (sa, 2H, 15), 2.41 (s, 3H, 17) ppm. **^{13}C NMR** (75MHz, $CDCl_3$): δ =125.50 (C1), 133.11 (C2), 127.35 (C3), 123.27 (C4), 137.95 (C5), 195.45 (C6), 109.01 (C7), 171.09 (C8), 131.97 (C9), 128.08 (C10), 129.29 (C11), 141.89 (C12), 129.29 (C13), 128.08 (C14), 32.32 (C15), 148.39 (C16), 21.52 (C17) ppm. **MS (EI)**: m/z (%) = 250 (20%). **HRMS** (FAB^+): calculated for $C_{17}H_{14}O_2$: 251.1072. Found: 251.1079.

Compound 4 ($C_{17}H_{14}O_3$, *M*=266 g/mol) was prepared starting from *o*-phthalaldehyde (0.5g, 3.7mmol), 4'-methoxyacetophenone (0.56g, 3.7 mmol) and NaOH (0.119g, 2.98mmol) and was obtained as a yellow solid, **mp**.112-114 °C, (0.7 g, 2.6 mmol, 71%). **IR**: ν 1601, 1566 cm^{-1}. **^{1}H NMR** (300 MHz, $CDCl_3$): δ= 15.33(s, 1H, OH), 7.47 (d, 1H, 1), 7.51 (dd, 1H, 2), 7.37 (dd, 1H,3), 7.82 (d, 1H, 4), 7.89 (d, 2H, 10, 14), 6.95 (d, 2H, 11, 13), 3.82 (s, 2H, 15), 3.83 (s, 3H, 17) ppm. **^{13}C NMR** (75MHz, $CDCl_3$): δ = 125.37 (C1), 132.85 (C2), 127.23 (C3), 123.03 (C4), 137.87 (C5), 194.84 (C6), 108.32 (C7), 170.04 (C8), 127.00 (C9), 129.99 (C10), 113.88 (C11), 162.06 (C12), 113.88 (C13), 129.99 (C14), 32.45 (C15), 148.09 (C16), 55.30 (C17) ppm. MS (EI): m/z (%) = 266 (15%). **HRMS** (FAB^+): calculated for $C_{17}H_{14}O_3$: 267.1021. Found: 267.1023.

General procedure for the synthesis of iron(III) complexes of 2-benzylidene-1-indanone derivatives

A solution of 2-benzylidene-1-indanone derivatives (compounds **1** to **4**) in anhydrous ethyl ether (20 mL) was treated with $Fe_2(CO)_9$ at room temperature for 2-3 h, under an inert atmosphere (Figure 2). After the reaction was complete, the crude product was filtered off through a Celite column, washed with ethyl ether and dissolved in dichloromethane. The solvent was evaporated to dryness. The iron complex (III) was obtained pure.

Compound 1a ($C_{48}H_{33}FeO_6$, *M*=761 g/mol) was prepared starting from 2-(phenylmethanone)-inden-1-ol (0.5 g, 2.1 mmol), and $Fe_2(CO)_9$ (0.31 g, 0.85 mmol) and was obtained as a purple solid, **mp**. 244-246°C, (0.425 g, 0.558 mmol, 80 %). **MS (FAB^+):** m/z (%) = 761 (2%). **HRMS** (FAB^+): calculated for $C_{32}H_{22}O_4Fe$ [M^+]: 526.0867. Found: 526.0877.

Compound 2a ($C_{48}H_{30}Cl_3FeO_6$, *M*=863 g/mol) was prepared starting from 2-(4-chlorophenylmethanone)-inden-1-ol (0.5g, 1.85 mmol), and $Fe_2(CO)_9$ (0.27 g, 0.74 mmol) and was obtained as a purple solid, **mp**. 232-234°C, (0.48 g, 0.55 mmol, 90%). **MS (FAB^+)**: m/z (%) = 864 (2%). **HRMS** (FAB^+): calculated for $C_{32}H_{20}O_4ClFe$ [M^+]: 594.0088. Found: 594.0092.

Compound 3a ($C_{51}H_{39}FeO_6$, *M*=803 g/mol) was prepared starting from 2-(4-methylphenylmethanone)-inden-1-ol (0.5 g, 2 mmol), and $Fe_2(CO)_9$ (0.29 g, 0.8 mmol) and was obtained as a purple solid, **mp**. 238-240 °C, (0.33 g, 0.4 mmol, 61%). **MS (FAB^+)**: m/z (%) = 803 (5%). **HRMS** (FAB^+): calculated for $C_{34}H_{26}O_4Fe$ [M^+]: 554.1180. Found: 554.1187.

Compound 4a ($C_{51}H_{39}FeO_9$, *M*=851 g/mol) was prepared starting from 2-(4-methoxyphenylmethanone)-inden-1-ol (0.5 g, 1.87 mmol), and $Fe_2(CO)_9$ (0.274 g, 0.75 mmol) and was obtained as a purple solid, **mp**. 234-236°C, (0.37 g, 0.43 mmol, 70%). **MS (FAB^+)**: m/z (%) = 851 (2%). **HRMS** (FAB^+): calculated for $C_{34}H_{26}O_6Fe$ [M^+]: 586.1079. Found: 554.1082.

Thin film deposition and characterization

Thin film deposition of iron(III) complexes with substituted 2-benzylidene-1-indanones was carried out by vacuum thermal evaporation. The material was deposited onto quartz and (100) single-crystalline silicon (c-Si) 200 Ω-cm wafers. The substrate temperatures were kept at 298 K during deposition. The evaporation source was a tungsten boat and the temperature through the tungsten boat was slowly increased to 498 K. The pressure in the vacuum chamber before the film deposition was $1x10^{-6}$ torr and the evaporation rate was 0.2 Å/s. The thickness measurements were made with a *Sloan Dektak IIA* profilometer on a quartz substrate. IR measurements were obtained with a Nicolet iS5-FT spectrophotometer, using silicon flakes as substrate for the thin films. For SEM, a *Leica Cambridge* scanning electron microscope (model *Stereoscan 440*) was coupled to a microanalysis system and operated at a voltage of 20 kV and a focal distance of 25 mm, using thin films on a quartz substrate. AFM characterization used a *JEOL* microscope, model *JSPM-4210*, with the *Tapping (AFM)* work mode. For AFM characterization of the films, quartz substrates were used. Ultraviolet-visible spectroscopy was carried out in a *Unicam* spectrophotometer, model *UV300*, with a quartz substrate.

Conclusions

We show an easy and fast method to synthesize 2-benzylidene-1-indanone derivatives and a new method to synthetize iron(III) complexes of 2-benzylidene-1-indanone derivatives was used to prepare semiconducting thin films. Thin films were prepared by a vacuum thermal evaporation process. The thermal evaporation

process had no effect on the intra-molecular bonds, suggesting that the chemical composition of the films did not change. Thin-film morphology seems to depend on the molecular structure. The chemical differences between the substituents in the complexes and the structural variations observed in the molecular-film arrangements provided a glimpse on the optical properties of these compounds. The optical transitions were found to be of a non-direct nature. The optical band gap was calculated and the values found were similar among all thin films. The optical absorption coefficients of iron(III) complexes of 2-benzylidene-1-indanone derivatives, as well as their optical band gaps, makes their thin films promising candidates for potential applications in solar cells or as emitting layers in OLEDs.

Acknowledgements

The authors wish to thank the technical assistance of M. Rivera (IF-UNAM), Rocío Patiño, Luis Velasco, Javier Pérez and IN4 (IQ- UNAM), as well as Guillermo Villagrán (Universidad Anáhuac). The authors gratefully acknowledge the financial support of the SEP-CONACYT-México, under project number 153751 and CONACYT project 127796 and DGAPA-PAPIIT project IN201212. We would also like to thank CONACYT for the Ph.D. grant extended to M. L.G.

Notes and references

[a] Instituto de Química, Universidad Nacional Autónoma de México. Circuito Exterior, Ciudad Universitaria, 04510, México, D. F.

[b] Universidad Anáhuac del Norte. Avenida Universidad Anáhuac núm. 46, Col. Lomas Anáhuac, C.P. 52786, Huixquilucan, Estado de México.

Electronic Supplementary Information (ESI) available: NMR and Mass Spectrometry data provided in attached files. See DOI: 10.1039/b000000x/

1 S. Rigaut, J. Massue, D. Touchard, J. L. Fillaut, S. Golhen and P. H. Dixneuf, *Angew. Chem. Int. Edit. Engl.,* 2002, **41**, 4513.

2 J. C. Röder, F. Meyer and E. Kaiser, *Angew. Chem. Int. Edit. Eng.,* 2002, **41**, 2304.

3 D. Astruc, *Acc. Chem. Res.*, 1997, **30,** 383.

4 R.A. Laudise, Ch. Kloc, P.G. Simpkins, T. Siegrist, *J. Crystal Growth*, 1998, **187,** 449.

5 Puigdollers, J.; Voz, C.; Orpella, A.; Martin, I.; Vetter, M.; Alcubilla, R. *Thin Solid Films,* 2003, **427,** 367.

6 M. E. Sánchez-Vergara, A. Ortiz, C. Álvarez-Toledano, José G. López-Cortés, A. Moreno, J. R. Álvarez, *Thin Solid Films*, 2008, **516,** 6382.

7 P. Cassoux, D. De Caro, L. Valade, H. Casellas, B. Daffos, M.E. Sánchez Vergara, *Mol. Cryst. Liq. Cryst*., 2002, **380,** 45.

8 J. Zabicky. *The Chemistry of Metal Enolates*, Part 1 (Patai Series), Wiley England, 2009.

9 a)V. Orlov, I. Borovoi and V. F. Lavrushin, *Zh. Obshch. Khim*., 1976, **17**, 691.b) V. Orlov, I. Borovoi, U. Surov and V. F. Lavrushin *Zh. Obshch. Khim.*, 1976, **46**, 2138. c) A. Hoser, Z. Laluski and H. Maluszynska, Acta Cryt. 1980, **B36**, 1258.

10 a)A.Saito, M. Umakoshi, N. Yagyu and Y. Hanzawa, Org. Lett., 2008, **10**, 1783. P. Wessig, C. Glombitza, G. Müller and J. Teubner, J. Org. Chem., 2004, **69**, 7582. b) Y.Wan, X.M. Chen, L.L. Pang, R. Ma, C. H. Yue,R. Yuan, W. Lin,R. Cheng Bo and H. Wu, *Synth. Commun.,*2010, **40**, 2320. c) C. Carrignon, P. Makowski, M. Antonietti and F. Goettman, *Tetrahedron Lett.*, 2009, **50**, 4833.

11 D. A. Thornton, *Coord. Chem. Rev*, 1990, **104,** 173.

12 H. C. Brown, *J. Am. Chem. Soc.,* 1957, **22,** 339.

13 a) M. L. Kantouri, T. Dimitriadis, C. D. Papadopoulos, M. G. Agnieszka Czapik, A. G. Hatzidimitriou, *Z. Anorg. Allg. Chem.*, 2009, **635,** 2185. b) S. M. Cohen, M. Meyer, K. N. Raymond, *J. Am. Chem. Soc.*, 1998, **120**, 6277

14 R.D. Hancock, D.A. Thornton, *Theoret. Chim. Acta (Berl.)***,** 1970, **18**, 67.

15 R. Seoudi, G.S. El-Bahy, Z.A. El Sayed, *Optical Materials* 2006, **29**, 304-312.

16 a) M.M. El-Nahass, M.M. Sallam, H.A. Ali, *International Journal of Modern Physics B*, 2005, **19**, 4057. b) M.M. El-Nahass, K.F. Abd-El-Rahman, A.A.A. Darwish. *Materials Chemistry and Physics,* 2005, **92**, 185-189.

17 A. Thakur, G. Singh, G.S.S. Saini, N. Goyal, S.K. Tripathi, *Optical Materials*, 2007, **30**, 565.

18 S. Adachi, *Optical Properties of Crystalline and Amorphous Semiconductors*, Kluwer Academic Publishers, Boston, 1999.

19 G.M. Sheldrick, *Acta Crystallog., Sect. A :Fundam. Crystallogr.,* 2008, **64,** 112.